Petrophysical Analysis of Geothermal Systems at Mount Meager, Southwestern British Columbia (Part of NTS 092J)

F. Hormozzade Ghalati[1], **Department of Earth Sciences, Carleton University, Ottawa, Ontario, fatemehormozzadeghal@cmail.carleton.ca**

J.A. Craven, Natural Resources Canada, Geological Survey of Canada–Central, Ottawa, Ontario

D. Motazedian, Department of Earth Sciences, Carleton University, Ottawa, Ontario

S.E. Grasby, Natural Resources Canada, Geological Survey of Canada–Calgary, Calgary, Alberta

Hormozzade Ghalati, F., Craven, J.A., Motazedian, D. and Grasby, S.E. (2024): Petrophysical analysis of geothermal systems at Mount Meager, southwestern British Columbia (part of NTS 092J); *in* Geoscience BC Summary of Activities 2023, Geoscience BC, Report 2024-01, p. 93–100.

Introduction

An essential aspect of geothermal energy utilization is the knowledge of factors influencing fluid flow pathways (Li, 2020). Fluid flow pathways are predominantly shaped by permeable geological elements, such as fractures, joints and faults, which are the key factors influencing the distribution of fluids within reservoirs and heat conduction in geothermal systems (Hanano, 2000). Researchers have employed diverse methods to investigate fluid flow pathways and their governing parameters in geothermal reservoirs. These methodologies involve numerical modeling (e.g., Strehlow et al., 2015), laboratory experiments and structural analyses (e.g., Farquharson et al., 2015; Eggertsson et al., 2020), geochemical studies (e.g., Libbey and Williams-Jones, 2016) and geophysical techniques (e.g., Heise et al., 2016; Cordell et al., 2019; Miller et al., 2022), each providing unique insights into flow pathways at various depths of investigation.

The Mount Meager Volcanic Complex (MMVC) in southwestern British Columbia (BC) stands as a prominent geothermal resource in Canada (Grasby et al., 2012). Its abundant thermal springs and high enthalpy geothermal potential (based on borehole temperature data) suggest the presence of permeable conduits channelling fluids to the near surface (Grasby et al., 2021). To expand the understanding of the potential geothermal reservoir beneath the MMVC, a comprehensive project was initiated in 2019, which includes a gravity survey, passive seismic analysis, deep and shallow magnetotelluric (MT) studies and bedrock mapping (Grasby et al., 2020, 2021, 2023).

The MT method is a passive electromagnetic exploration technique that measures the magnetic and electric fields on the Earth's surface (Chave and Jones, 2012). Natural electromagnetic signals span a broad frequency range of 0.001 to 40 000 hertz (Hz). The audio-magnetotelluric (AMT) method measures the natural electromagnetic fields at the higher frequencies (1 to 40 000 Hz), which permits mapping of relatively shallower subsurface electrical resistivity structures than those mapped by the MT method. Electrical resistivity, a fundamental physical property influenced by factors such as pore geometry, rock composition, fluid content and temperature, offers a means of reservoir assessment in geothermal systems (Muñoz, 2014). Resistivity models derived from the inversion of MT data enable the modelling of subsurface structures by analyzing natural perturbations in the Earth's electric and magnetic fields. Prior MT studies at Mount Meager identified a deep magma body beneath the volcano and its possible connection to the geothermal system (Jones and Dumas, 1993; Candy, 2001; Hanneson and Unsworth, 2022). A more comprehensive dataset, gathered using the AMT method in 2019, explores subsurface structures within the top hundred metres and up to a few kilometres beneath the MMVC (Figure 1; Craven et al., 2020).

This project establishes empirical relationships between laboratory petrophysical data (porosity and permeability) and the AMT-derived resistivity model. The goal is to comprehensively assess the spatial relationships between geological structures and fluid circulation within the potential geothermal reservoir beneath the MMVC.

Study Area

Mount Meager (an active volcano within the Garibaldi volcanic belt) is situated about 150 km north of Vancouver, BC, and displays rugged topography forged through uplift and erosion over the past 2.5 million years (Figure 1; Huang, 2019). Its geological composition predominantly

[1] *The lead author is a 2023 Geoscience BC Scholarship recipient.*

This publication is also available, free of charge, as colour digital files in Adobe Acrobat® PDF format from the Geoscience BC website: https://geosciencebc.com/updates/summary-of-activities/.

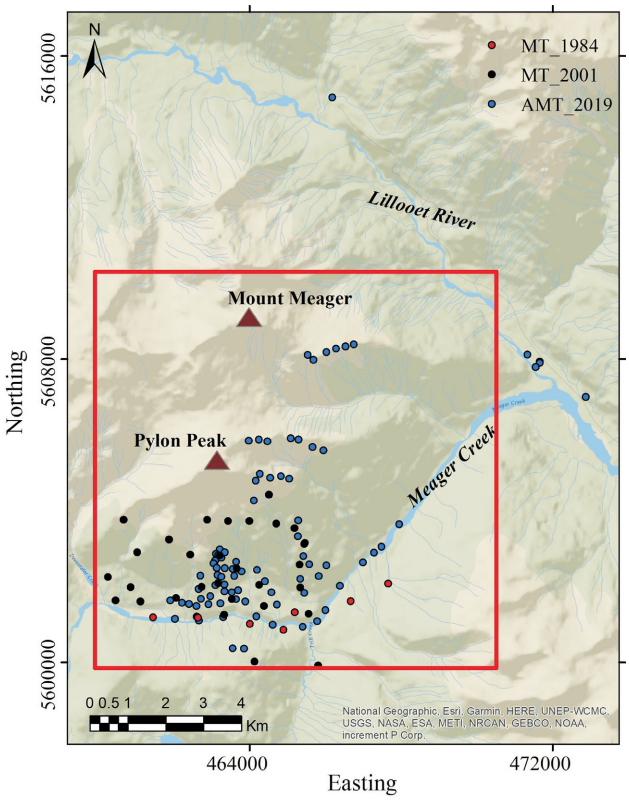

Figure 1. Overview of the Mount Meager Volcanic Complex study area. Locations of the magnetotelluric (MT) / audio-magnetotelluric (AMT) stations are shown. The 1984 MT stations are from Jones and Dumas (1993) and the 2001 MT stations are from Candy (2001). The red outlined area is shown in Figure 2. All co-ordinates are in UTM Zone 10N, NAD 83.

features Mesozoic fractured crystalline and metamorphic rocks, including quartz diorite, granodiorite, dacite and gneiss. The hydraulic conductivity and permeability at Mount Meager primarily depend on fracture porosity, as evidenced by observed fluid loss during drilling of the basement rock. Furthermore, the distribution of upward fluid flow is influenced by fault and fracture zones, dikes and hydrothermal brecciation associated with volcanic activities (Adams and Moore, 1987).

Notable fault zones within the MMVC region include the Meager Creek fault (MCF), No-Good fault (NGF), Camp fault and Carbonate fault. The MCF, a key structure in controlling the geothermal system, exhibits an east-striking normal fault with an approximately 45–50° northward dip. It plays a sealing role, preventing fluid flow across the fault, and is considered the southern boundary of the reservoir. The NGF, Camp and Carbonate faults intersect the MCF and exhibit varying strike directions and dips, adding complexity to the fault system (Figure 2). Additionally, steeply dipping regional fractures and local fractures contribute to the structural heterogeneity of the MMVC's granodiorite (Balfour et al., 2011).

The distribution of thermal springs in southwestern BC is linked to major crustal-scale faults that provide permeable pathways for hot water seepage to the surface. These springs are spatially correlated with fractured rocks dissected by faults. For example, the Meager Creek hot springs discharge hot water due to a topographic rise in the

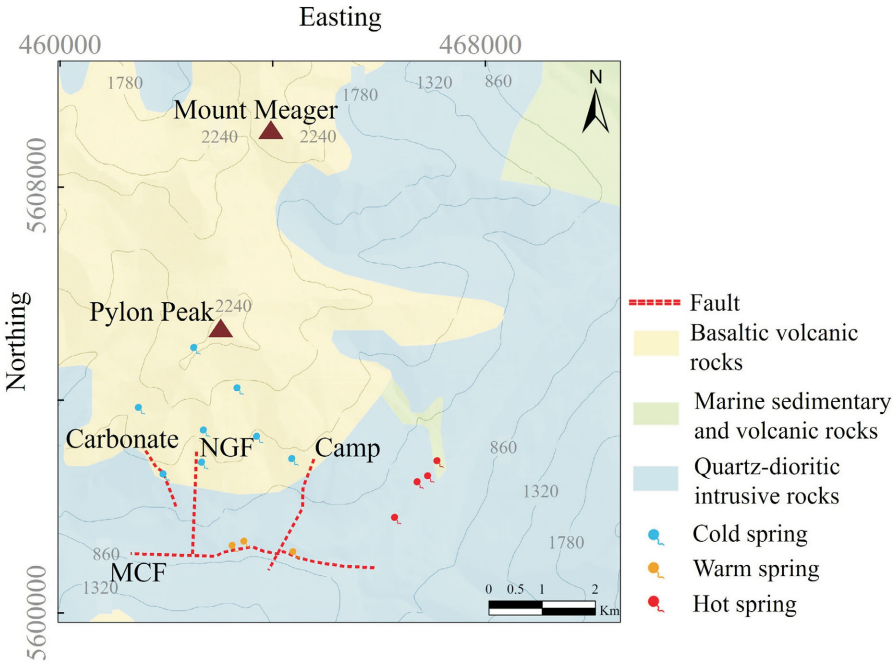

Figure 2. Geological map of the Mount Meager Volcanic Complex. Background geology modified after Proenza (2012). Elevations are shown as contour lines (in m asl) and all co-ordinates are in UTM Zone 10N, NAD 83. Abbreviations: Camp, Camp fault; Carbonate, Carbonate fault; MCF, Meager Creek fault; NGF, No-Good fault.

bedrock, whereas warm springs align with the trace of the MCF, indicative of permeable zones allowing thermal fluid outflow (Jamieson, 1981; Bernard, 2020; Hormozzade Ghalati et al., 2022).

Data and Methodology

Understanding fluid flow in a reservoir depends on the rocks' physical properties, including porosity, permeability and pore connectedness. Porosity reflects the volume of pore space in a medium, whereas permeability measures the medium's capacity to allow fluid flow (Bernabé et al., 2010). Evaluating these fundamental properties is essential in assessing hydraulic conductivity and flow characteristics within a geothermal reservoir.

This project analyzed 21 surface core samples collected from various locations within the MMVC, including both volcanic and basement rocks. Porosity and permeability were measured using the Coretest Systems, Inc. AP-608 Gas combined permeameter and porosimeter at the Institut national de la recherche scientifique (INRS; Québec, Quebec). Additionally, aside from rock matrix porosity, fracture porosity was identified in the studied rocks. Quantitative insight into the impact of fractures on porosity and permeability was gained by employing theoretical models that consider various fracture attributes. The characteristics of these fractures, including dip angle, dip direction, orientation, length, spacing and aperture, were essential in assessing the fracture networks. Fracture data were collected from surface outcrops in the study area at locations where fresh bedrock was exposed. Fracture porosity (φ_f; fraction) is calculated as

$$\varphi_f = w_f \times \left(\frac{1}{D_i} + \frac{1}{D_j} \right), \quad (1)$$

where w_f is fracture aperture (m), and D is spacing (m) in i and j directions. Moreover, permeability through a set of fractures (k_f in mD; 1 millidarcy = 9.869233×10^{-16} m^2) can be expressed using the following equation, where the fracture aperture is in µm and porosity is in % (Tiab and Donaldson, 2016):

$$k_f = 8.33 \times 10^{-4} \times w_f \times \varphi_f \quad (2)$$

Moreover, porosity relates to the electrical resistivity of bulk rock and fluid. This relationship can be defined through petrophysical models like Archie's law (Equation 3; Archie, 1942), modified Archie's law (MAL; Equation 4; Glover et al., 2000), Hashin Shtrikman (HS) model (Equation 5; Hashin and Shtrikman, 1962) and Waxman Smits model (Waxman and Smits, 1968).

$$\sigma_f = \sigma_b \varphi^{-m} \quad (3)$$

$$\sigma_b = \sigma_f \varphi^m + \sigma_s \ (1-\varphi)^p \quad (4)$$

$$p = \frac{\log\ (1-\varphi^m)}{\log\ (1-\varphi)}$$

$$\sigma_s + \frac{\varphi}{\frac{1}{\sigma_f - \sigma_s} + \frac{1-\varphi}{3\sigma_s}} = \sigma_b^{HS-} \le \sigma_b \le \sigma_b^{HS+} = \sigma_f + \frac{1-\varphi}{\frac{1}{\sigma_s - \sigma_f} + \frac{\varphi}{3\sigma_f}} \quad (5)$$

In these equations, φ is porosity, m is an empirical constant for the cementation factor, σ_b is the bulk electrical conductivity of the hostrock (Siemens/metre [S/m]), σ_f is the fluid electrical conductivity (S/m), σ_s is the solid phase conductivity of the material (S/m), HS^+ is the upper Hashin-Shtrikman bound of the bulk electrical conductivity and HS^- is the lower Hashin-Shtrikman bound of the bulk electrical conductivity. These models help in defining porosity at the locations where the electrical conductivity measurements are available.

In addition to petrophysical data, geophysical data provides valuable insights into the composition and physical properties of rocks and fluids around boreholes. To expand the understanding of rock properties on a larger scale, the AMT method was used to infer subsurface electrical resistivity. The impedance tensor (Z; Equation 6; Chave and Jones, 2012) and geomagnetic transfer function (or tipper, T; Equation 7; Simpson and Bahr, 2005) were employed to interpret resistivity structures. The Z defines a relationship between the horizontal components of the Earth's electric (Ex and Ey) and magnetic (H_x and H_y) fields considering the angular frequency (ω). The T defines the relationship between the horizontal (H_x and H_y) and vertical (H_z) components of the Earth's magnetic field.

$$\begin{bmatrix} E_x \\ E_y \end{bmatrix} = \begin{bmatrix} Z_{xx} & Z_{xy} \\ Z_{yx} & Z_{yy} \end{bmatrix} \begin{bmatrix} H_x \\ H_y \end{bmatrix} \quad (6)$$

$$H_z(\omega) = (T_x(\omega) \quad T_y(\omega)) \begin{pmatrix} H_x(\omega) \\ H_y(\omega) \end{pmatrix} \quad (7)$$

Additionally, temperature, pressure, and geological logs are available for all boreholes in this project. The combination of geochemical, petrophysical and geophysical data sources contribute significantly to the comprehensive assessment of the MMVC's subsurface properties and fluid dynamics.

Results

The results of the 3-D AMT data inversion and petrophysical evaluation of the MMVC is published in Hormozzade

Ghalati et al. (2022, 2023). An overview of the published results is provided here.

The final model was acquired after 35 iterations and a root mean square (RMS) of 1.4 using CGG's RLM-3D modelling code (Soyer et al., 2018). Most of the stations have an overall RMS misfit of less than one, which shows the acceptance of the model.

The main features in the model include two major conductors (C1 and C2), which exhibit an average resistivity of around 15 ohm (Ω)·m and are embedded within a background resistivity of approximately 100 Ω·m. These relatively shallow conductive zones are interpreted to represent the low-permeability clay-rich layers found in various boreholes; layers that maintain measured temperatures ranging from 70 to 160 °C. These clay-rich layers function as caprocks, enabling the accumulation of deeper fluids. Within the boreholes, the shallow conductive zones are associated with argillic alteration minerals, characterized by the presence of smectite, illite and, occasionally, kaolinite (Hormozzade Ghalati et al., 2023).

The geological structures influencing thermal activity in the Mount Meager region are the MCF and NGF, which have east-west and north-south orientations, respectively. According to this AMT resistivity model, surfaces inclined at angles of 50–60° and 80–90° are representative of the MCF and NGF, respectively. These angles align with available structural geology data. In this model, the intersection of the NGF and MCF corresponds to conductive zones and potential paths for fluid movement (Figure 3). This correlation is substantiated by noticeable changes in electrical resistivity occurring at the fault locations. The average electrical resistivity of the pathways in the AMT model is between 40 and 300 Ω·m. These resistivity shifts are evident along the western and southern boundaries of the model, coinciding with the fault indications represented by the planes and lines in Figure 3.

In order to assess the fluid pathways shown within the AMT model using petrophysical models (Equations 3 to 5), the initial step involved computing the electrical resistivity of the fluid samples from boreholes and thermal springs. Due to the effects of temperature on electrical resistivity, the fluid sample resistivities were adjusted to the reservoir temperature using Equation 8:

$$R_{wT2} = R_{wT1}\left(\frac{T1+x}{T2+x}\right) \qquad (8)$$

$$x = 10^{-((0.3404 \times \log_{10} R_{wT1}) - 0.6414)},$$

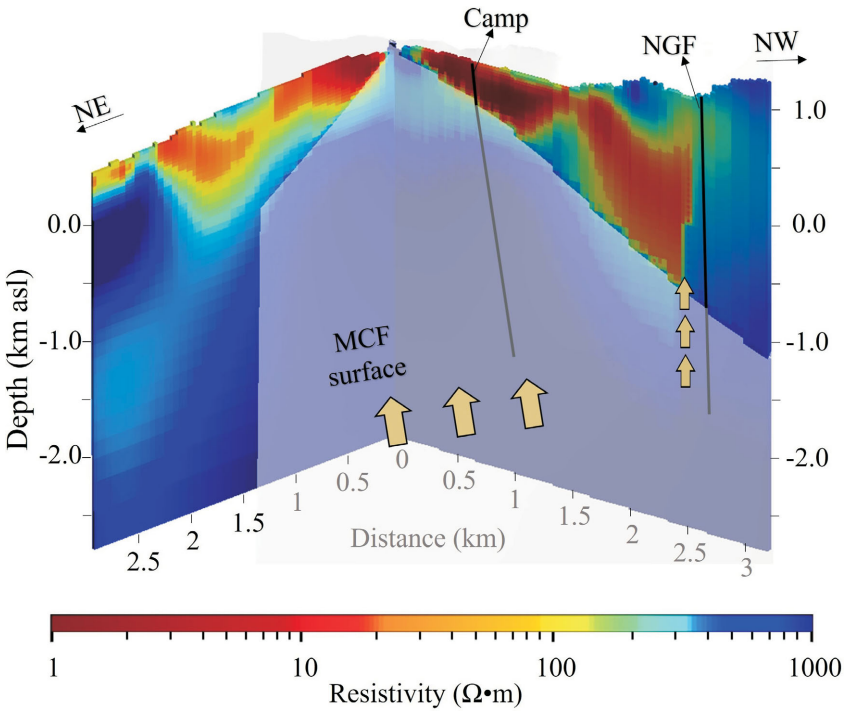

Figure 3. Cross-sectional view through the 3-D electrical resistivity model of the southern part of Pylon Peak (Hormozzade Ghalati et al., 2023). Local faults (Meager Creek fault [MCF], Camp fault [Camp] and No-Good fault [NGF]) are illustrated as surfaces. Yellow arrows show the potential direction of fluid flow. The view for these sections is from the north, hence east corresponds to the left of the figures, and west corresponds to the right. Abbreviation: Ω, ohm; NE, northeast; NW, northwest.

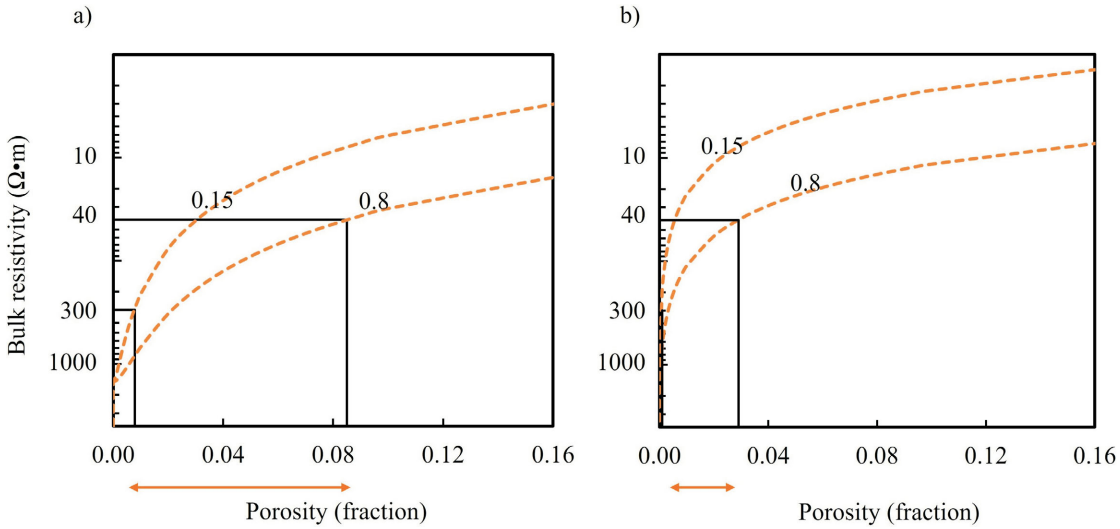

Figure 4. Interpretation of the electrical resistivity model of the Mount Meager Volcanic Complex. Dashed lines show different fluid resistivities with the fluid resistivity values annotating the lines. The changes in fluid resistivity between 0.15 and 0.8 Ω·m are highlighted. The fluid fraction is estimated for the potential reservoir zone, using **a)** modified Archie's law (MAL) and **b)** an upper Hashin and Shtrikman bound (HS^+). A two-phase medium with a pore connectedness of 1.6 and hostrock conductivity of 0.0007 Siemens/metre (S/m) is assumed to define the electrical resistivity versus porosity.

where R_{wT1} and R_{wT2} are the electrical resistivity (Ω·m) of the fluid at temperatures of T1 and T2 in °C (Tiab and Donaldson, 2016). Fluid resistivity calculations show a range of values from 0.15 to 0.80 Ω·m for the borehole fluid samples at the reservoir temperature. These corrected electrical resistivity values were then used in further porosity-permeability calculations. Considering the MAL and HS models, a porosity range of 0.1–8.5% is expected for the range of bulk electrical resistivity obtained from the AMT model (Figure 4).

Taking into account the porosity-permeability relationship based on laboratory measurements of the MMVC rock samples, it is anticipated that the permeability for the indicated fluid pathways of the AMT model falls within the range of 0 to 0.249 mD (0 to 2.46×10^{-16} m^2). For natural geothermal convection at reservoir temperatures ranging from 200 to 250 °C, a permeability on the order of 1.01 mD (9.97×10^{-16} m^2) is typically required (as indicated by Straus and Schubert, 1977). However, as the temperature increases, resulting in a reduction in fluid viscosity, the minimum permeability needed for fluid flow can be lowered to around 0.1 mD (9.97×10^{-17} m^2), particularly at higher reservoir temperatures (350 °C; e.g., Hanano, 2000). Because permeability measurements of the core samples depend on the physical sample size, macroscopic fractures might not be captured and considered in the studied core samples. Moreover, the geology mainly consists of Mesozoic fractured crystalline and metamorphic rocks and fractures were detected by high amounts of fluid loss during drilling of the basement rocks. Therefore, fracture networks at the MMVC should be studied. Fracture porosity and permeability was calculated for surface fracture data (Equations 1 and 2). It was estimated that the porosity and permeability of the fracture zones can increase up to 40% and 666 mD (6.57×10^{-13} m^2), respectively.

Summary

This paper summarizes the integration of laboratory core measurements of porosity and permeability and fluid chemistry data with the 3-D electrical resistivity model. This integrated approach enabled the development of new petrophysical models linking porosity and permeability to electrical resistivity. By calibrating these models using well log and laboratory-based rock physical data, porosity and permeability values were derived from the resistivity model. Moreover, potential fracture zones within the study area were characterized, which helped in explaining the permeable pathways governing the upflow of thermal fluids within the Mount Meager Volcanic Complex.

The Mount Meager Volcanic Complex was studied due to the abundance of historical data, which is attributed to the presence of warm and hot springs, pre-existing drilled boreholes and nearby communities that are enthusiastic about embracing alternative energy sources. The outcomes of this research enhance the understanding of the geological aspects of geothermal resources and will contribute to the broader objectives of mitigating the economic risks associated with geothermal exploration within the Garibaldi volcanic belt.

Acknowledgments

This project was funded by Natural Resources Canada and Geoscience BC and benefited from support of the Natural

Sciences and Engineering Research Council of Canada through Carleton University. The authors would like to thank S.M. Ansari for reviewing this manuscript. The authors would also like to thank E. Roots for providing pyMT code; V. Tschirhart, R. Bryant and S.M. Ansari for helping during the field survey; T. Jenkins from the Lil'wat First Nation for ensuring wildlife were undisturbed; M. Accurrso, D. Vincent and R. Slinger for piloting (No Limits Helicopters); and Innergex Renewable Energy Inc. for providing significant access to their field bunkhouse. The authors also thank Meager Creek Development Corporation for providing water chemistry data and CGG for providing RLM-3D and Geotools software.

References

Adams, M.C. and Moore, J.N. (1987): Hydrothermal alteration and fluid geochemistry of the Meager Mountain Geothermal System, British Columbia; American Journal of Science, v. 287, no. 7, p. 720–755.

Archie, G.E. (1942): The electrical resistivity log as an aid in determining some reservoir characteristics; Transactions of the AIME, v. 146, no. 1, p. 54–62, URL <https://doi.org/10.2118/942054-G>.

Balfour, N.J., Cassidy, J.F., Dosso, S.E. and Mazzotti, S. (2011): Mapping crustal stress and strain in southwest British Columbia; Journal of Geophysical Research, v. 116, art. B03314, 11 p., URL <https://doi.org/10.1029/2010JB008003>.

Bernabé, Y., Li, M. and Maineult, A. (2010): Permeability and pore connectivity: a new model based on network simulations; Journal of Geophysical Research, v. 115, art. B10203, 14 p., URL <https://doi.org/10.1029/2010JB007444>.

Bernard, K. (2020): Epithermal clast coating inside the rock avalanche-debris flow deposits from Mount Meager Volcanic Complex, British Columbia (Canada); Journal of Volcanology and Geothermal Research, v. 402, art. 106994, URL <https://doi.org/10.1016/j.jvolgeores.2020.106994>.

Candy, C. (2001): Crew development corporation report on a magnetotelluric survey, South Meager geothermal project, Pemberton, British Columbia; Frontier Geosciences Inc., unpublished report for Frontier Geosciences project FG1-581.

Chave, A.D. and Jones, A.G. (2012): The Magnetotelluric Method: Theory and Practice; Cambridge University Press, New York, New York, 552 p., URL <https://www.cambridge.org/core/books/magnetotelluric-method/magnetotelluric-method/C7110AAC1567259EC65172C35B5F16EA> [October 2023].

Cordell, D., Unsworth, M.J., Diaz, D., Reyes-Wagner, V., Currie, C.A. and Hicks, S.P. (2019): Fluid and melt pathways in the central Chilean subduction zone near the 2010 Maule earthquake (35–36 °S) as inferred from magnetotelluric data; Geochemistry, Geophysics, Geosystems, v. 20, no. 4, p. 18–35, URL <https://doi.org/10.1029/2018GC008167>.

Craven, J.A., Hormozzade, F., Tschirhart, V., Ansari, M., Bryant, R. and Montezadian, D. (2020): Overview of the 2019 audiomagnetotelluric survey of the Mount Meager geothermal reservoir; Chapter 6 *in* Garibaldi Geothermal Energy Project, Mount Meager 2019 - Field Report, Geoscience BC, Report 2020-09, p. 126–147, URL <https://www.geosciencebc.com/i/project_data/GBCReport2020-09/GeoscienceBCReport%202020-09.pdf> [March 2021].

Eggertsson, G.H., Lavallée, Y., Kendrick, J.E. and Markússon, S.H. (2020): Improving fluid flow in geothermal reservoirs by thermal and mechanical stimulation: the case of Krafla volcano, Iceland; Journal of Volcanology and Geothermal Research, v. 391, art. 106351, URL <https://doi.org/10.1016/j.jvolgeores.2018.04.008>.

Farquharson, J., Heap, M.J., Varley, N.R., Baud, P. and Reuschlé, T. (2015): Permeability and porosity relationships of edifice-forming andesites: a combined field and laboratory study; Journal of Volcanology and Geothermal Research, v. 297, p. 52–68, URL <https://doi.org/10.1016/j.jvolgeores.2015.03.016>.

Glover, P.W.J., Hole, M.J. and Pous, J. (2000): A modified Archie's law for two conducting phases; Earth and Planetary Science Letters, v. 180, no. 3, p. 369–383, URL <https://doi.org/10.1016/S0012-821X(00)00168-0>.

Grasby, S.E., Allen, D.M., Bell, S., Chen, Z., Ferguson, G., Jessop, A., Kelman, M., Ko, M., Majorowicz, J., Moore, M., Raymond, J. and Therrien, R. (2012): Geothermal energy resource potential of Canada; Geological Survey of Canada, Open File 6914, 322 p., URL <https://doi.org/10.4095/291488>.

Grasby, S.E., Ansari, S.M., Barendregt, R.W., Borch, A., Calahorrano-DiPatre, A., Chen, Z., Craven, J.A., Dettmer, J., Gilbert, H., Hanneson, C., Harris, M., Hormozzade, F., Leiter, S., Liu, J., Muhammad, M., Quane, S.L., Russell, J.K., Salvage, R.O., Savard, G., Tschirhart, V. et al. (2021): Garibaldi Geothermal Energy Project – phase 1 – final report; Geoscience BC, Report 2021–08, 276 p., URL <https://www.geosciencebc.com/i/project_data/GBCReport2021-08/GBCR%202021-08%20Garibaldi%20Geothermal%20Energy%20Project%20-%20Phase%201.pdf> [February 2022].

Grasby, S.E., Ansari, S.M., Calahorrano-Di Patre, A., Chen, Z., Craven, J.A., Dettmer, J., Gilbert, H., Hanneson, C., Harris, M., Liu, J., Muhammad, M., Russell, K., Salvage, R.O., Savard, G., Tschirhart, V., Unsworth, M.J., Vigouroux-Caillibot, N. and Williams-Jones, G. (2020): Geothermal resource potential of the Garibaldi volcanic belt, southwestern British Columbia (part of NTS 092J); *in* Geoscience BC Summary of Activities 2019: Energy and Water, Geoscience BC, Report 2020-02, p. 103–108, URL <https://www.geosciencebc.com/i/pdf/SummaryofActivities2019/EW/Project%202018-004_EW_SOA2019.pdf> [February 2022].

Grasby, S.E., Borch, A., Calahorrano-Di Patre, A., Chen, Z., Craven, J., Liu, X., Muhammad, M., Russell, J.K., Tschirhart, V., Unsworth, M.J., Williams-Jones, G. and Yuan, W. (2023): Garibaldi Geothermal Volcanic Belt Assessment Project, southwestern British Columbia (part of NTS 092J), phase 2: 2022 field report; *in* Geoscience BC Summary of Activities 2022: Energy and Water, Geoscience BC, Report 2023-02, p. 47–54, URL <https://www.geosciencebc.com/i/project_data/GBCReport2023-02/P2018-004_Grasby_EnergyWaterSoA2022.pdf> [October 2023].

Hanano, M. (2000): Two different roles of fractures in geothermal development; *in* Proceedings of the World Geothermal Congress 2000, May 28–June 10, 2000, Kyushu-Tohoku, Japan, International Geothermal Association, p. 2597–2602.

Hanneson, C. and Unsworth, M. (2022): Magnetotelluric investigations of geothermal systems centred in southern British

Columbia (parts of NTS 082, 083, 092, 093); *in* Geoscience BC Summary of Activities 2021: Energy and Water, Geoscience BC, Report 2022-02, p. 81–94, URL <https://www.geosciencebc.com/i/pdf/SummaryofActivities2021/EW/Sch_Hanneson_EWSOA2021.pdf> [October 2023].

Hashin, Z. and Shtrikman, S. (1962): A variational approach to theory of effective magnetic permeability of multiphase materials; Journal of Applied Physics, v. 33, no. 10, p. 3125–3131, URL <https://doi.org/10.1063/1.1728579>.

Heise, W., Caldwell, T.G., Bertrand, E.A., Hill, G.J., Bennie, S.L. and Palmer, N.G. (2016): Imaging the deep source of the Rotorua and Waimangu geothermal fields, Taupo Volcanic Zone, New Zealand; Journal of Volcanology and Geothermal Research, v. 314, p. 39–48, URL <https://doi.org/10.1016/j.jvolgeores.2015.10.017>.

Hormozzade Ghalati, F., Craven, J.A., Motazedian, D., Grasby, S.E., Roots, E., Tschirhart, V., Chen, Z. and Liu, X. (2023): Analysis of fluid flow pathways in the Mount Meager Volcanic Complex, southwestern Canada, utilizing AMT and petrophysical data; Geochemistry, Geophysics, Geosystems, v. 24, no. 3, art. e2022GC010814, 20 p., URL <https://doi.org/10.1029/2022GC010814>.

Hormozzade Ghalati, F., Craven, J.A., Motazedian, D., Grasby, S.E. and Tschirhart, V. (2022): Modeling a fractured geothermal reservoir using 3-D AMT data inversion: insights from Garibaldi volcanic belt, British Columbia, Canada; Geothermics, v. 105, art. 102528, URL <https://doi.org/10.1016/j.geothermics.2022.102528>.

Huang, K. (2019): Geochemical analysis of thermal fluids from southern Mount Meager, British Columbia, Canada; M.Sc. thesis, University of Iceland, 92 p.

Jamieson, G.R. (1981): A preliminary study of the regional groundwater flow in the Meager Mountain geothermal area, British Columbia; M.Sc. thesis, The University of British Columbia, 163 p., URL <http://hdl.handle.net/2429/22494> [May 2020].

Jones, A.G. and Dumas, I. (1993): Electromagnetic images of a volcanic zone; Physics of the Earth and Planetary Interiors, v. 81, p. 289–314, URL <https://doi.org/10.1016/0031-9201(93)90137-X>.

Li, J. (2020): Investigations of fluid flow through fractures in enhanced geothermal systems; Ph.D. thesis, University of Queensland, 127 p., URL <https://doi.org/10.14264/uql.2020.973>.

Libbey, R.B. and Williams-Jones, A.E. (2016): Compositions of hydrothermal silicates and carbonates as indicators of physicochemical conditions in the Reykjanes geothermal system, Iceland; Geothermics, v. 64, p. 15–27, URL <https://doi.org/10.1016/j.geothermics.2016.04.007>.

Miller, C.A., Barretto, J., Stagpoole, V., Caratori-Tontini, F., Brakenrig, T. and Bertrand, E. (2022): The integrated history of repeated caldera formation and infill at the Okataina Volcanic Centre: insights from 3D gravity and magnetic models; Journal of Volcanology and Geothermal Research, v. 427, art. 107555, URL <https://doi.org/10.1016/j.jvolgeores.2022.107555>.

Muñoz, G. (2014): Exploring for geothermal resources with electromagnetic methods; Surveys in Geophysics, v. 35, no. 1, p. 101–22, URL <https://doi.org/10.1007/s10712-013-9236-0>.

Proenza, Y. (2012): Geothermal data compilation and analysis of Alterra Power's upper Lillooet property; M.Eng. thesis, University of British Columbia, 47 p., URL <https://www.geosciencebc.com/i/project_data/GBC2017-006/Yuliana%20Proenza%20MEng%20Project.zip> [September 2023].

Simpson, F. and Bahr, K. (2005): Practical Magnetotellurics; Cambridge University Press, Cambridge, United Kingdom, 270 p., URL <https://www.cambridge.org/core/books/practical-magnetotellurics/FB76CCD1DB4A49AB48429A22E7D4E5D8> [October 2023].

Soyer, W., Mackie, R. and Miorelli, F. (2018): Optimizing the estimation of distortion parameters in magnetotelluric 3d inversion; 80th EAGE Conference and Exhibition, June 11–14, 2018, Copenhagen, Denmark, European Association of Geoscientists & Engineers, v. 2018, p. 1–5, URL <https://doi.org/10.3997/2214-4609.201801399>.

Straus, J.M. and Schubert, G. (1977): Thermal convection of water in a porous medium: effects of temperature- and pressure-dependent thermodynamic and transport properties; Journal of Geophysical Research, v. 82, p. 325–333, URL <https://doi.org/10.1029/JB082i002p00325>.

Strehlow, K., Gottsmann, J.H. and Rust, A.C. (2015): Poroelastic responses of confined aquifers to subsurface strain and their use for volcano monitoring; Solid Earth Discussions, v. 7, no. 2, p. 1673–1729, URL <https://doi.org/10.5194/sed-7-1673-2015>.

Tiab, D. and Donaldson, E.C. (2016): Naturally fractured reservoirs; Chapter 8 *in* Petrophysics (4th edition), Gulf Professional Publishing, Boston, Massachusetts, p. 415–481, URL <https://doi.org/10.1016/B978-0-12-803188-9.00008-5>.

Waxman, M.H. and Smits, L.J.M. (1968): Electrical conductivities in oil-bearing shaly sands; Society of Petroleum Engineers Journal, v. 8, no. 2, p. 107–122.